Advances in Water Resources 71 (2014) 16–22

Contents lists available at ScienceDirect

Advances in Water Resources

journal homepage: www.elsevier.com/locate/advwatres

Optimal root profiles in water-limited ecosystems ☆

Keith Rudd [a], John D. Albertson [b,*], Silvia Ferrari [a]

[a] Department of Mechanical Engineering and Materials Science, Duke University, Durham, NC 27707, USA
[b] Department of Civil and Environmental Engineering, Duke University, Durham, NC 27707, USA

ARTICLE INFO

Article history:
Received 4 September 2013
Received in revised form 11 April 2014
Accepted 23 April 2014
Available online 4 May 2014

Keywords:
Root distribution
Kalahari
Richards equation
Ecosystem hydraulic dynamics

ABSTRACT

The vertical distribution of roots in the soil is of central importance to the mass and energy exchange between the land and the atmosphere. It has been demonstrated that the vertical root profiles which maximize transpiration in numerical experiments reflect well the characteristics of root profiles observed in nature for water-limited ecosystems. Previous research has demonstrated how the optimal vertical root profile depends on both the mean annual precipitation (MAP) and the soil texture. Recently, in the climate literature, it has been suggested Chou et al. (2012) [5] that increased greenhouse forcing in the tropics can lead to a simultaneous decrease in the frequency and increase in the intensity of precipitation. In this paper we demonstrate how such a change in the statistical structure of rainfall, even with no change to MAP, requires deeper root distributions to maintain optimal water use. These results raise interesting questions for future studies of nutrient dynamics, the cost of additional below ground carbon allocation, and inter plant functional type competition.

1. Introduction

A plant's growth, reproduction, and survival all depend on the plant's ability to absorb soil moisture through its root system [17,18]. As root distributions are controlled by the survival strategy of the plant, optimization concepts have been used to identify ideal root distributions based on ecohydrological facets of the soil–plant–atmosphere system [19]. In this paper we focus on water-limited ecosystems and identify vertical root profiles that maximize transpiration in order to explore how potential shifts in the temporal structure of rainfall might affect competition between different rooting strategies, as well as how herbaceous plants would need to adjust their root profile to remain optimal in its access to water.

Knowledge of the active root layer is essential for the study of water and nutrient dynamics as needed in atmospheric science, hydrology, ecology, and geochemistry (e.g. Bhattachan et al. [2]). There are several factors that influence root depths and distributions. For example, Schenk and Jackson found a positive correlation between rooting depths and annual potential evapotranspiration (*PET*), mean annual precipitation (MAP), and length of the warm season [28]. In particular, Schenk and Jackson were able to use MAP to explain 62% of the observed variance in median rooting depths for herbaceous plants in water-limited ecosystems [29].

It has also been shown that root distributions [12] and absolute root depths [3] vary by vegetation type. As mentioned above, Schenk and Jackson found a positive correlation between MAP and median root distributions for herbaceous plants [28,29], however, Bhattachan et al. showed that this correlation may not apply to woody root distributions [2].

The primary role of roots is soil water extraction to support transpiration at the leaf surface as occurs during photosynthesis. Therefore, one can think of the optimal root system as one which best supports photosynthesis.

Kleidon and Heimann [14] estimated optimal root depths by maximizing the carbon gain to the vegetation within a global Terrestrial Biosphere Model. Schwinning and Ehleringer explored potential trade-offs in water uptake and carbon cost by developing a simple model of plant water transport and carbon gain in a two-layered soil environment [30]. Similarly, Guswa provided a cost-benefit analysis of root structures [10,11], where the optimal root depth was balanced by the carbon cost of forming the root structure.

In the case of water-limited ecosystems total transpiration is a useful optimization target. Transpiration optimality was first used to predict root characteristics in [25], where Protopapas and Bras identified root profiles that maximize transpiration in a maize crop in Flevoland (Netherlands). They used a transient soil moisture model to examine inter-storm dynamics (i.e. extended drought

☆ This paper is based upon work sponsored by the IGERT WISeNet NSF Grant #DGE-1068871 and by the NSF Hydrologic Sciences program Grant #NSF-0838301.
* Corresponding author. Tel.: +1 919 660 5468.
E-mail address: john.albertson@duke.edu (J.D. Albertson).

http://dx.doi.org/10.1016/j.advwatres.2014.04.021
0309-1708/

period). A similar approach was taken in [6], where Collins and Bras explored the effects of soil texture and rainfall seasonality on rooting depths. van Wijk employed this approach and demonstrated that observed patterns of rooting characteristics of herbaceous plant species could be explained using the concept of hydrological optimality for arid climates [37]. In [16] Laio et al. used an analytical model of soil moisture to link vertical root distributions to climate and soil properties. Specifically, they investigated the dependency of the optimal average root depth on average daily rainfall and potential transpiration (PT) for various soil types. Sivandran and Bras also used optimal transpiration to investigate the relationship between soil type and optimal root profiles in [32]. In their analysis they used a stochastic rainfall model to generate rainfall data for a single climate.

Recent analysis of the climate system [5] has suggested that increased greenhouse forcing can lead to mechanistic changes in precipitation frequency and intensity. In fact, there is a likely tendency towards decreased frequency and increasing intensity in the tropics [5]. This raises the question of how root profiles may need to adapt to simultaneous changes in storm depth and frequency. ith this as motivation we depart from the approach in previous efforts (e.g. [6,16,25,32,37]) and we focus on how changes to the statistical structure of rainfall would affect the "optimal root profiles." We use Richards' equation to model soil moisture forced by seasonally varying potential evapotranspiration (PET), leaf area index (LAI), and rainfall statistics. As this work focuses on water-limited ecosystems, we use transpiration as a proxy for carbon gain (e.g. [39]) and we do not consider possible effects of nutrient limitation [20]. We also assume in our analysis that there is no plant interaction with the water table.

For each climate type and trial root profile, Richards equation is solved using a new constrained integration (CINT) partial differential equation (PDE) solution method. The CINT method is similar to pseudo-spectral solution methods; in this method traditional Galerkin methods are combined with a modified constrained backpropagation (CPROP) [9,22] algorithm in which radial basis functions (RBFs) are used to enforce the boundary conditions.

This paper is organized as follows: Section 2 gives a mathematical description of the governing equations used in the model. Section 3 describes the climate and soil types used in the mathematical simulations. The results of the simulations are given in Section 4, followed by a brief discussion in Section 5.

2. Model description

We model the transient state of soil moisture that is driven at the surface by rain and evaporative demand. In this model, roots compete for moisture with evaporative effects near the soil surface and with gravity drainage at lower depths. It is assumed that interception is negligible, though the consideration of interception would not change the analyses, rather it would effect the rainfall distribution as described in [27]. It is also assumed that rainfall rates in excess of the maximum infiltration rate are lost as runoff. Additionally, we consider only vertical water fluxes and assume that the root zone does not interact directly with the water table below. The variables and parameters used in the model are summarized in Table 1.

Soil moisture within the vadose zone was modeled using Richards' equation [4]:

$$\frac{\partial\theta}{\partial t}(z,t) = \frac{\partial}{\partial z}\left\{K[\psi(z,t)]\left[\frac{\partial\psi}{\partial z}(z,t)+1\right]\right\} - S(z,t). \tag{1}$$

The soil moisture, $\theta(z,t)$, and matric potential, $\psi(z,t)$, states are related here by van Genuchten's formula [34],

$$\theta(\psi) = \theta_r + (\theta_s - \theta_r)S_e(\psi), \tag{2}$$

Table 1
Description of model variables and parameters.

Variable	Description
z	Vertical distance (positive up) [cm]
t	Time [d]
ψ	Matric Potential [cm]
θ	Volumetric water content [cm ^{3}/cm ^{3}]
K	Hydraulic conductivity [cm/d]
S	Root sink term [d^{-1}]
r	Precipitation rate [cm/d]
E	Evaporation [cm/d]
T	Total transpiration
ρ	Root density [1/cm]
γ	Root efficiency term
PET	Potential evapotranspiration [cm/d]
PE	Potential evaporation [cm/d]
PT	Potential transpiration [cm/d]
LAI	Leaf area index [m^2/m^2]
θ_r	Residual water content [cm^3/cm^3]
θ_s	Saturated water content [cm^3/cm^3]
α	Fitting parameter [cm^{-1}]
n	Fitting parameter (dimensionless)
m	Fitting parameter (dimensionless)
k_s	Saturated soil conductivity [cm/d]
ℓ	Fitting parameter (dimensionless)

where

$$S_e(\psi) = [1 + (\alpha\psi)^n]^{-m}. \tag{3}$$

The hydraulic conductivity, K, was approximated using Mualem's formula [21],

$$K(\psi) = k_s S_e^{\ell}(\psi)\left[1 - \left(1 - S_e^{1/m}(\psi)\right)^m\right]^2. \tag{4}$$

The values used for the soil parameters pertaining to the soil types used are shown in Table 2.

The sink term, $S(z,t)$, is the rate at which moisture is extracted from the soil by the root system at time t and depth z, and is described by

$$S = \gamma(\psi)\rho(z)PT, \tag{5}$$

where $\gamma(\psi)$, shown in Fig. 1, is the root efficiency term given by van Genuchten [36]

$$\gamma(\psi) = \frac{1}{1 + (\psi/\psi_{50})^p}. \tag{6}$$

In the above equation, ψ_{50} is the soil–water pressure head at which the extraction rate is reduced by 50%, and in the work presented in this paper was given the value of 50 cm, similar to values reported in [38]. The parameter p is commonly assumed to have a value of 3 (dimensionless) [35].

PET is partitioned into potential evaporation, PE, and potential transpiration, PT [26],

$$PE = PET(e^{-\sigma LAI}) \tag{7}$$

$$PT = PET(1 - e^{-\sigma LAI}), \tag{8}$$

Table 2
Soil specific parameters used in (2) and (4).

	Sandy loam	Sandy clay loam
θ_s	.41	.39
θ_r	.065	.1
α	−.075	−.059
n	1.89	1.49
m	$1-n$	$1-n$
ℓ	.5	.5
k_s	106.1	31.44

where $\sigma = .4$ [6]. Seasonal *LAI*, with values similar to those reported in [13,24], was represented by,

$$LAI(t) = 1 + \tanh(3\cos(2\pi t/365)). \tag{9}$$

A plot of (9) is shown in Fig. 2. We also assume seasonal *PET*, with a peak daily total of 5 mm/d during the wet/growing season and 1.25 mm/d during the dry season [33]. This is represented by

$$PET(t) = .5\pi[3/8(1 + \cos(2\pi t/365)) + .25] \times \max\{\sin(2\pi t), 0\}. \tag{10}$$

We use an analytical function of shape for the root density, given by

$$\rho(z) = \frac{c(z/D_{50})^{c-1}}{D_{50}\left[1 + (z/D_{50})^{c}\right]^2}, \tag{11}$$

where c is defined as

$$c = \frac{2.94}{\ln(D_{50}/D_{95})}. \tag{12}$$

D_{50} and D_{95} are parameters that determine the shape of $\rho(z)$. D_{50} determines the depth at which the bulk of the root density is located; specifically, it is the depth above which 50% of the root is located. The parameter D_{95} is associated with absolute rooting depths, and is the depth above which 95% of the root is located. This density function is the derivative of the cumulative density function proposed by Schenk and Jackson [28] and has been widely used to describe root distributions of herbaceous plants [6,37]. An example density is shown in Fig. 3 for $D_{50} = -100$ [cm] and $D_{95} = -200$ [cm].

Since previous efforts have focused on the impact of changes In MAP on the rooting depth, in this work study how, for fixed MAP, varying storm frequency and intensity affect the optimal root profile. We focus on relative changes in root distribution rather than absolute rooting depth, and so, it was assumed that $D_{95} = -200$ [cm] in order to simplify the analysis. The parameter D_{50} was allowed to vary to maximize the total transpiration,

$$T = \int_0^{10\times 365} \int_{-400}^{0} S(z,t)\, dz\, dt. \tag{13}$$

A 10 year period was chosen as the time frame for each simulation, as this was deemed suitable to sample well the statistical structure of rainfall and also ensure a duration long enough to be meaningful for plant competition.

The boundary condition at the surface ($z = 0$) is given as a specified flux (Neumann condition) [4] using Darcy's law

$$r(t) - E[\psi(0,t)] = K(\psi)\left(\frac{\partial\psi}{\partial z} + 1\right)\Big|_{z=0}, \tag{14}$$

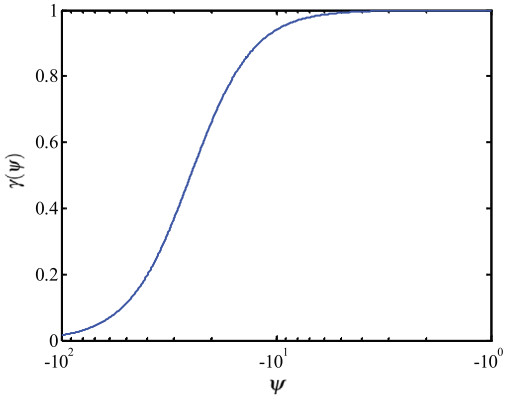

Fig. 1. Root efficiency, $\gamma(\psi)$, as a function of matric potential, ψ.

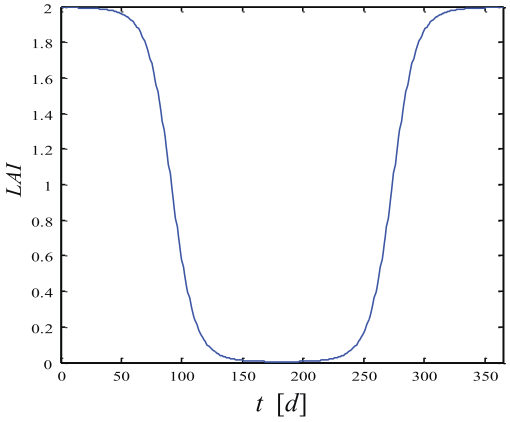

Fig. 2. Seasonal structure of *LAI* as a function of t [24].

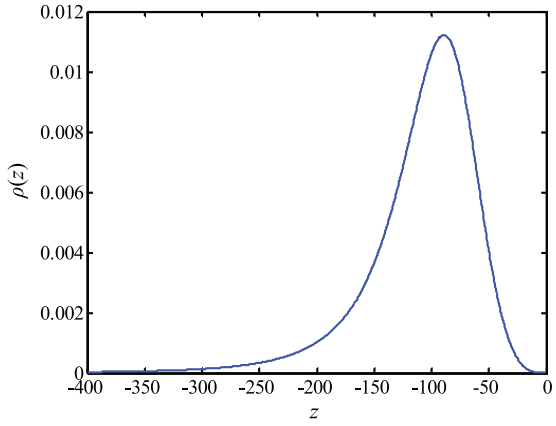

Fig. 3. Example root density profile, $\rho(z)$, with $D_{50} = -100$ and $D_{95} = -200$.

where $r(t)$ is the rainfall rate and $E[\psi(0,t)]$ is the soil evaporation rate given by

$$E = \beta[S_e(\psi(0,t))]PE. \tag{15}$$

In the above equation, *PE* is the potential evaporation specified by (8) and $\beta[S_e(\psi(0,t))]$ is a function that describes the effect of water stress on soil evaporation. The water stress function ranges from 0 to 1, and in this study is assumed to have the form

$$\beta[S_e(\psi(0,t))] = \frac{1}{2}\left[1 + \tanh\left(c_2 S_e^{c_3} - \frac{c_1}{S_e}\right)\right]_{z=0}, \tag{16}$$

where c_1, c_2, and c_3 are positive constants. A plot of $\beta[S_e(\psi(0,t))]$ is shown in Fig. 4. Note that this function's output is similar to piecewise functions commonly used (see [6,37]), however is differentiable everywhere.

We seek to examine modest perturbations in key features of a climate's precipitation structure. A two parameter stochastic rainfall generator was used to obtain the rainfall time series used in these simulations. With this generator, precipitation is represented as a Marked Poisson process with mean storm frequency, λ^* [d^{-1}], and mean storm depth α^* [mm] [7,8,10,27].

The boundary condition at the bottom of the soil profile, taken to be at $z = -400$ cm, is given by drainage under gravity (e.g. [1]) and was implemented by enforcing

$$\frac{\partial\psi}{\partial z}\Big|_{z=-400} = 0. \tag{17}$$

Richards' equation (1) was solved using the CINT method [15]. The CINT method is similar to pseudo-spectral solution methods; in this method traditional Galerkin methods are combined with a

modified CPROP algorithm [9,22], in which RBFs are used to enforce the boundary conditions. The CINT method was chosen because it has been shown to be faster and more accurate than the finite element (FE) method for several types of PDEs [15]. A summary of the CINT method and its application to Richards' equation (1) is included in Appendix A.

3. Experimental setup

While others have previously examined the relationship between MAP and rooting depth, in this paper we focus on the effects of simultaneous changes in storm frequency and intensity on the optimal vertical root distributions. This section specifies climate and soil properties that were used in the model description given in the previous section. We use the Kalahari Transect [39] as an interesting example, but the work is intended to illuminate the general case of changing precipitation structure in water-limited ecosystems.

3.1. Affect of precipitation on root depth

For each sampled combination of rain frequency and intensity, forcing series were generated for eleven year periods. Mean storm frequency was varied from 0.1 to 0.4 d^{-1}, and mean depth varied from 8 to 12 mm of precipitation, similar to values reported by Porporato et al. [23] for a transect of the Kalahari. Storm frequency, λ^*, was allowed to vary seasonally,

$$F_m = [.5(1+\tanh(\cos(2\pi m/12))]^4, \tag{18}$$

$$\lambda_m = \lambda^* F_m/\overline{\mathbf{F}}, \tag{19}$$

$$\lambda_m^* = \min\{\lambda_m, .99\}. \tag{20}$$

where m indicates the month of year, and λ_m^* is the average storm frequency for month m. The average depth was also allowed to vary seasonally,

$$\alpha_m^* = \alpha^* + 3.5\tanh(\cos(2\pi m/12+\pi)). \tag{21}$$

From the eleven year period, the first year was used for 'spin-up' to minimize the effects of the initial conditions. Simulations were then run over the remaining 10 years for analysis. The soil type used in these numerical experiments was sandy loam, and the parameters associated with this soil are given in the following subsection.

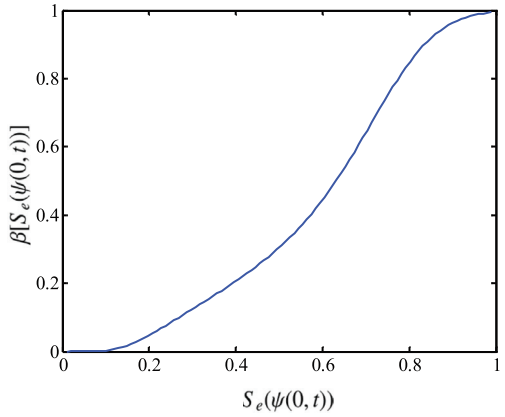

Fig. 4. Water stress function $\beta[S_e(\psi(0,t))]$ used to approximate the rate of evaporation.

3.2. Sensitivity to underlying soil type

We also explore the sensitivity of our results to underlying soil type by obtaining the optimal root profiles for two different soil types. In these simulations we look at the wet end of the Kalahari, near Mongu Zambia, with mean storm depth $\alpha^* = 10.1$ mm and mean arrival time $\lambda^* = .38\ d^{-1}$ [23]. The average monthly totals for this site are plotted in Fig. 5, and are in close agreement with the monthly averages reported in [23].

The two soil types considered in this work were sandy loam and sandy clay loam. The parameters associated with these soil types are found in Table 2.

4. Simulations and results

4.1. Variable storm type

The results of the simulations across storm types are given in Figs. 6–9. These figures were included in order to give a complete picture of how the other water fluxes are effected by shifting storm types. The contour lines in these figures show constant values of MAP. In Fig. 6 the optimal D_{50} is shown over the range of values of λ^* and α^* that were explored. These results indicate that for low MAP the optimal profile is distributed closer to the surface, and becomes more deeply distributed as MAP increases, as shown in [6,16,25,32,37]. This suggest that, for areas with low MAP, plants compete with evaporation for water. However, as MAP increases, the roots must compete with evaporation and drainage for moisture and, hence, a deeper distribution becomes advantageous.

The novel contribution of this study is the analysis of how the optimal root structure may change with the distribution of rainfall, without requiring a shift in MAP. In these findings we provide a view of below ground implications for possible changes in α^* and λ^* [5]. Following any contour line of constant MAP in Fig. 6, we observe that as frequency decreases and depth increases, deeper roots are advantageous.

The average yearly transpiration, drainage, and evaporation in the simulations with optimal root profiles (Fig. 6) are shown in Figs. 7–9. Change in storage is not included for brevity, as it was small (on the order of the observed error). These figures show that transpiration, drainage, and evaporation remain nearly constant along lines of constant MAP, provided the vegetation is able to adapt to the new storm frequency and intensity.

4.2. Variable soil type

The results of the simulations over varying soil types are shown in Figs. 10–12. Fig. 10 shows simulated transpiration as a function

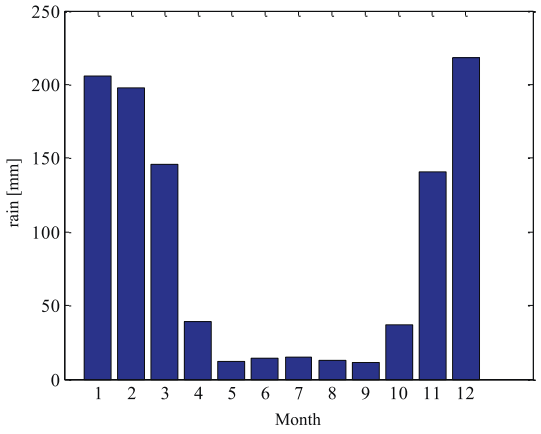

Fig. 5. Average monthly rainfalls generated for $\alpha^* = 10.1$ mm and $\lambda^* = .38\ d^{-1}$.

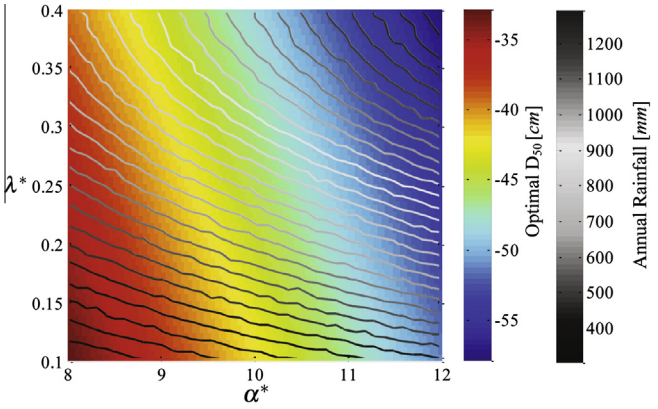

Fig. 6. Optimal value of D_{50} versus mean storm depth, α^*, and mean arrival time, λ^*.

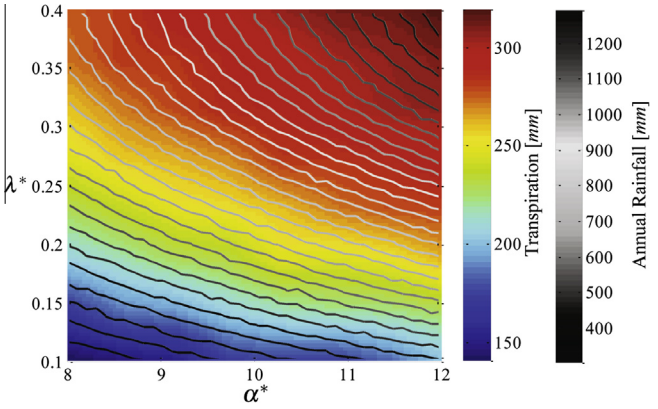

Fig. 7. Mean annual transpiration as a function of mean storm depth, α^*, and mean arrival time, λ^*.

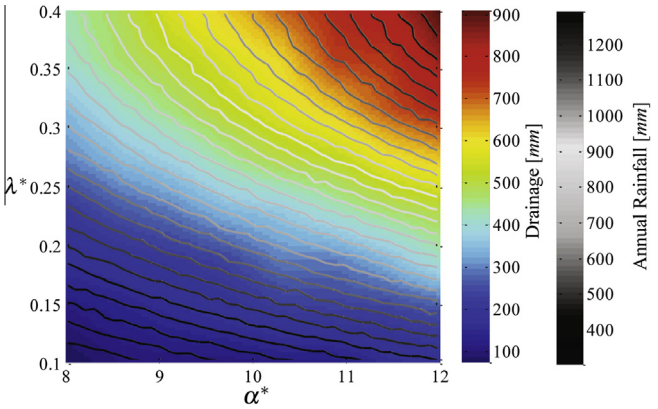

Fig. 8. Mean annual drainage as a function of mean storm depth, α^*, and mean arrival time, λ^*.

of D_{50} for the two soil types used in this study, where the optimal D_{50} has been indicated. Fig. 11 shows the simulated drainage, and Fig. 12 shows the simulated evaporation. The corresponding optimal profiles for each soil are shown in Fig. 13. We see, as others have observed (see [6,16,32,37]), that for soils with high conductivity, the optimal profile is more deeply distributed. This characteristic also agrees with what has been observed in nature [12,29].

5. Discussion

The results in the previous section demonstrate that more well-drained soils call for more deeply distributed optimal root profiles,

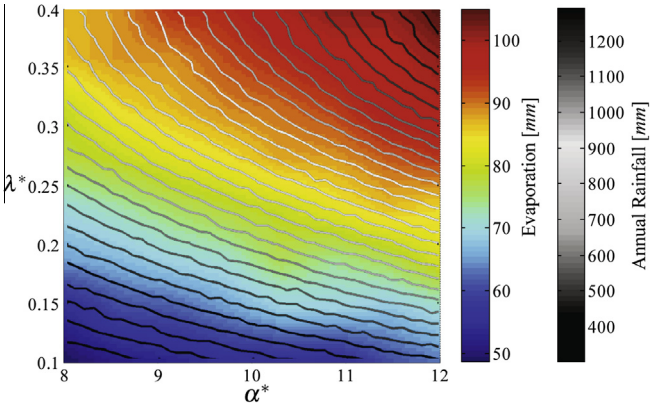

Fig. 9. Mean annual evaporation as a function of mean storm depth, α^*, and mean arrival time, λ^*.

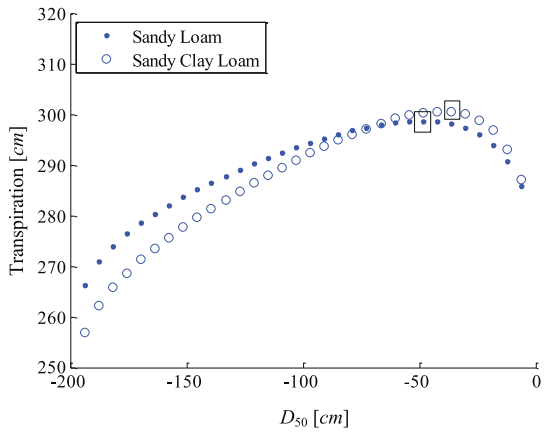

Fig. 10. Mean annual transpiration vs. D_{50} for each soil type. Note that boxes are inserted to identify the optimal value for each soil type.

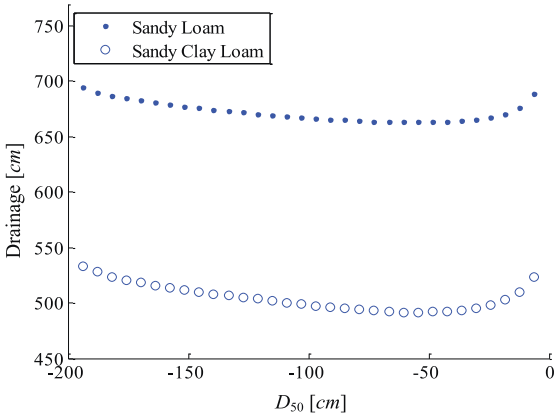

Fig. 11. Mean annual drainage vs. D_{50} for each soil type.

as observed in nature [12,29]. These results are in agreement with previous work [6,16,25,32,37]. The water balances shown in Figs. 10–12 suggest that for sandier soils evaporative effects are not as significant as the effects of gravity, and, thus, a deeper distribution is optimal.

The results given for optimal profiles (Fig. 6) as a function of storm intensity and frequency show the dependence of the optimal profile on mean annual precipitation. These results agree with what was reported in [29], that root systems tend to be deeper

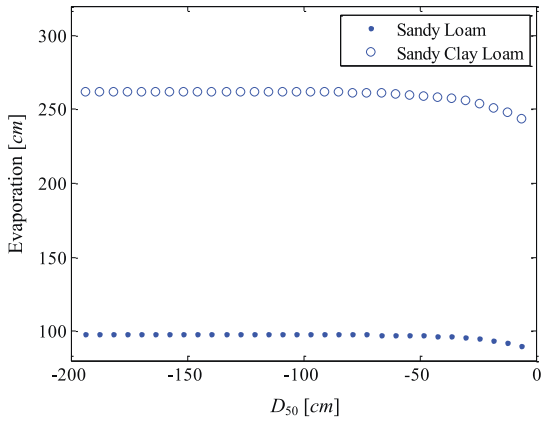

Fig. 12. Mean annual soil evaporation vs. D_{50} for each soil type.

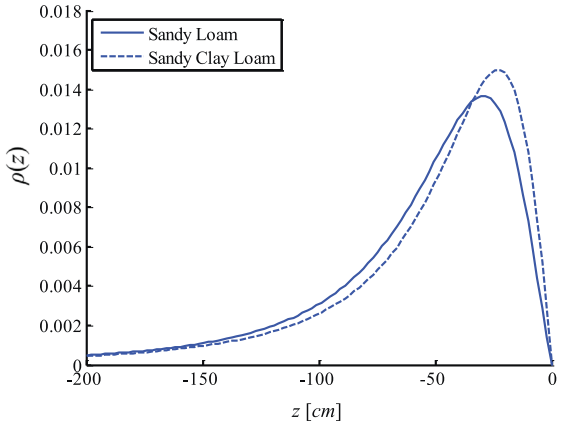

Fig. 13. Optimal root profiles for each soil type.

and narrower in cold and wet climates and more shallowly distributed in hot, dry climates.

The results shown in Fig. 6 demonstrate that as storms become less frequent and more intense, the optimal profile has a deeper distribution. It is interesting to note that the optimal profile regulates approximately the same water balance for each rainfall structure, suggesting that in order to maintain current rates of transpiration, plants may need to adjust rooting strategies in response to predicted climatic changes [5].

These results raise interesting questions for future studies of nutrient dynamics, the cost of additional below ground carbon allocation and inter plant functional type competition.

6. Conclusion

This work further advances the approach of studying optimal root distributions with a lense on maximizing transpiration use of soil water for water-limited ecosystems.

The optimal root profiles were identified for a spectrum of storm types, with mean depths ranging from 8 to 12 mm and mean frequencies ranging from .1 to .4 d^{-1}. It was shown that the optimal profile depends, not only on mean annual precipitation, but also on the storm type. These results suggest that as forcing from greenhouse gases result in shifting storm structure [5], plants in water limited ecosystems will be required to adapt their rooting strategies in order to maintain optimality and water balances. In particular, if tropical areas see decreased precipitation frequency and increased intensity, as suggested by [5], then there will be a needed investment in below ground carbon allocation to push deeper rooting systems to maintain optimal water use strategies.

Appendix A. Numerical solution

We have developed a constrained integration (CINT) method [15] for solving initial boundary value PDEs. The CINT method combines classical Galerkin methods with a constrained backpropogation (CPROP) training approach in order to constrain the artificial neural network (ANN) to approximately satisfy the boundary condition at each stage of integration.

To ease the numerical implementation in the application of the CINT method to Richards' equation, particularly near saturation, the substitution $\tilde{\psi}(z,t) = \log[-\psi(z,t)]$ was made. This substitution changes the PDE (1) to

$$\frac{\partial\tilde{\psi}}{\partial t}\frac{\partial\theta}{\partial\psi} = \frac{\partial\tilde{\psi}}{\partial z}\frac{\partial K}{\partial\psi}\left[1-\exp(\tilde{\psi})\frac{\partial\tilde{\psi}}{\partial z}\right] + K\left[\left(\frac{\partial\tilde{\psi}}{\partial z}\right)^2 + \frac{\partial^2\tilde{\psi}}{\partial z^2}\right] + \exp(-\tilde{\psi})S. \tag{A.1}$$

Note that the boundary condition at the bottom of the soil profile given in (17) does not change, as

$$\frac{\partial\psi}{\partial z} = -\exp(\tilde{\psi})\frac{\partial\tilde{\psi}}{\partial z} \tag{A.2}$$

implies that the boundary condition for the re-scaled hydraulic pressure head is

$$\left.\frac{\partial\tilde{\psi}}{\partial z}\right|_{z=-400} = 0. \tag{A.3}$$

The depth, z, was rescaled and shifted to $\tilde{z}$,

$$\tilde{z} = z/200 + 1, \tag{A.4}$$

so that $\tilde{z}\in[-1,1]$.

As done in Galerkin and pseudo-spectral methods, the re-scaled hydraulic pressure head, $\tilde{\psi}(\tilde{z},t)$, is approximated by the linear combination of basis functions,

$$\tilde{\psi}(\tilde{z},t) \approx \sum_{j=1}^{J}\phi_j(\tilde{z})\alpha_j(t). \tag{A.5}$$

The boundary condition (A.3) is enforced by setting

$$\alpha_1(t) = -\left(\frac{\partial\phi_1(\tilde{z})}{\partial\tilde{z}}\right)^{-1}\sum_{j=2}^{J}\frac{\partial\phi_j(\tilde{z})}{\partial\tilde{z}}\alpha_j(t)\Big|_{\tilde{z}=-1} \tag{A.6}$$

In the above equation, $\phi_1(z)$ is the Gaussian function

$$\phi_1(z) = \exp[-100(z+1.1)^2]. \tag{A.7}$$

For PDE problems that do not contain traveling waves, commonly used basis functions such as Fourier or Chebyshev polynomials can be used for $\phi_j(\tilde{z})$, however, as traveling waves appear in solutions to (1), piecewise cubic polynomials were found to be more effective. Letting the domain, $[-1,1]$ be partitioned into $J-1$ equally spaced subregions $[\tilde{z}_j,\tilde{z}_{j+1}]$, the functions $\phi_j(\tilde{z})$ for $j=2,\ldots,J$ are piecewise cubic polynomials given in (A.8), where $h=\tilde{z}_{j+1}-\tilde{z}_j$.

To solve Richards' equation, the right hand side of (A.6) is substituted into (A.5), giving an approximate solution that satisfies the boundary condition at the bottom of the soil profile. This approximate solution is then substituted into (A.1), and evaluated at collocation points within the domain $[-1,1]$, resulting in a system of ordinary differential equations (ODEs). This system of ODEs is then integrated to obtain an approximate solution to (A.1). In this work, the integration algorithm of choice was Matlab's *ODE15s* [31]. At each integration time step, t_j, the approximate solution

was re-constructed at the collocation points by evaluating (A.5). The approximate solution was then adjusted at the soil surface so as to satisfy the boundary condition (15), using fixed point iterations to deal with the nonlinearity in the condition.

$$\phi_j = \frac{1}{h^3}\begin{cases} (\tilde{z}-\tilde{z}_{j-2})^3, & \text{if } z \in [\tilde{z}_{j-2}, \tilde{z}_{j-1}] \\ h^3 + 3h^2(\tilde{z}-\tilde{z}_{j-1}) + 3h(\tilde{z}-\tilde{z}_{j-1})^2 - 3(\tilde{z}-\tilde{z}_{j-1})^3, & \text{if } \tilde{z} \in [\tilde{z}_{j-1}, \tilde{z}_j] \\ h^3 + 3h^2(z_{j+1}-z) + 3h(\tilde{z}_{j+1}-\tilde{z})^2 - 3(\tilde{z}_{j-1}-\tilde{z})^3, & \text{if } \tilde{z} \in [\tilde{z}_j, \tilde{z}_{j+1}] \\ (\tilde{z}_{j+2}-\tilde{z})^3, & \text{if } \tilde{z} \in [\tilde{z}_{j+1}, \tilde{z}_{j+2}] \\ 0, & \text{otherwise} \end{cases} \tag{A.8}$$

References

[1] Albertson JD, Kiely G. On the structure of soil moisture time series in the context of land surface models. J Hydrol 2001;243(12):101–19.

[2] Bhattachan Abinash, Tatlhego Mokganedi, Dintwe Kebonye, O'Donnell Frances, Caylor Kelly K, Okin Gregory S, Perrot Danielle O, Ringrose Susan, D'Odorico Paolo. Evaluating ecohydrological theories of woody root distribution in the Kalahari. PLoS ONE 2012;7(3):03.

[3] Canadell J, Jackson RB, Ehleringer JR, Mooney HA, Sala OE, Schulze E-D. Maximum rooting depth of vegetation types at the global scale. Oecologia 1996;108(4):583–95.

[4] Cesanelli Andrés, Guarracino Luis. Estimation of actual evapotranspiration by numerical modeling of water flow in the unsaturated zone: a case study in buenos aires, argentina. Hydrogeol J 2009;17(2):299–306.

[5] Chou Chia, Chen Chao-An, Tan Pei-Hua, Chen Kuan Ting. Mechanisms for global warming impacts on precipitation frequency and intensity. J Clim 2012;25(9):3291–306.

[6] Collins DBG, Bras RL. Plant rooting strategies in water-limited ecosystems. Water Resour Res 2007:43.

[7] Edoardo Daly A, Oishi Christopher, Porporato Amilcare, Katul Gabriel G. A stochastic model for daily subsurface {CO2} concentration and related soil respiration. Adv Water Resour 2008;31(7):987–94.

[8] Laio F, Porporato A, Ridolfi L, Rodriguez-Iturbe I. Plants in water-controlled ecosystems: active role in hydrologic processes and response to water stress – II. Probabilistic soil moisture dynamics. Adv Water Resour 2001;24(7).

[9] Ferrari S, Jensenius M. A constrained optimization approach to preserving prior knowledge during incremental training. IEEE Trans. Neural Networks 2008; 19(6):996–1009.

[10] Guswa AJ. The influence of climate on root depth: a carbon cost-benefit analysis. Water Resour Res 2008;44(2).

[11] Guswa AJ. Effect of plant uptake strategy on the wateroptimal root depth. Water Resour Res 2010;46(9).

[12] Jackson RB, Canadell J, Ehleringer JR, Mooney HA, Sala OE, Schulze ED. A global analysis of root distributions for terrestrial biomes. Oecologia 1996;108: 389–411.

[13] Jolly William M, Running Steven W. Effects of precipitation and soil water potential on drought deciduous phenology in the Kalahari. Global Change Biol 2004;10(3):303–8.

[14] Kleidon Axel, Heimann Martin. A method of determining rooting depth from a terrestrial biosphere model and its impacts on the global water and carbon cycle. Global Change Biol 1998;4(3):275–86.

[15] Rudd K, Ferrari S. A constrained integration (cint) approach to solve partial differential equations with artificial neural networks. Neurocomputing, submitted for publication.

[16] Laio F, D'Odorico P, Ridolfi L. An analytical model to relate the vertical root distribution to climate and soil properties. Geophys Res Lett 2006;33.

[17] Lee CA, Lauenroth WK. Spatial distributions of grass and shrub root systems in the shortgrass steppe. Am Midl Nat 1994;132(1):117–23.

[18] Lynch J. Root architecture and plant productivity. Plant Physiol 1995;109(1): 7–13.

[19] Mäkelä A, Givnish TJ, Berninger F, Buckley TN, Farquhar GD, Hari P. Challenges and opportunities of the optimality approach in plant ecology. Silva Fenn 2002;36(3):605–14.

[20] Rondena R, Albertson JD, Montaldo N, Mancini M. Parsimonious modeling of vegetation dynamics for ecohydrologic studies of water-limited ecosystems. Water Resour Res 2005;41(10).

[21] Mualem Yechezkel. A new model for predicting the hydraulic conductivity of unsaturated porous media. Water Resour Res 1976;12(3):513–22.

[22] Di Muro G, Ferrari S. A constrained-optimization approach to training neural networks for smooth function approximation and system identification. In: Proc. International Joint Conference on Neural Networks. Hong Kong; 2008.

[23] Porporato Amilcare, Laio Francesco, Ridolfi Luca, Caylor Kelly K, Rodriguez-Iturbe Ignacio. Soil moisture and plant stress dynamics along the Kalahari precipitation gradient. J Geophy Res: Atmos 2003;108(D3).

[24] Privette JL, Myneni RB, Knyazikhin Y, Mukelabai M, Roberts G, Tian Y, Wang Y, Leblanc SG. Early spatial and temporal validation of MODIS LAI product in the southern africa Kalahari. Remote Sens Environ 2002;83(1):232–43.

[25] Protopapas Angelos L, Bras Rafael L. A model for water uptake and development of root systems. Soil Sci 1987;144(5).

[26] Ritchie Joe T. Model for predicting evaporation from a row crop with incomplete cover. Water Resour Res 1972;8(5):1204–13.

[27] Rodriguez-Iturbe I, Porporato A, Ridolfi L, Isham V, Coxi DR. Probabilistic modelling of water balance at a point: the role of climate, soil and vegetation. Proc R Soc London Ser A: Math Phys Eng Sci 1999;455(1990):3789–805.

[28] Schenk HJ, Jackson RB. The global biogeography of roots. Ecol Monogr 2002; 72:311–28.

[29] Schenk HJ, Jackson RB. Rooting depths, lateral root spreads and below-ground/ above-ground allometries of plants in water-limited ecosystems. J Ecol 2002;90:480–94.

[30] Schwinning Susanne, Ehleringer James R. Water use trade-offs and optimal adaptations to pulse-driven arid ecosystems. J Ecol 2001;89(3):464–80.

[31] Shampine L, Reichelt M. The Matlab ODE suite. SIAM J Sci Comput 1997;18(1): 1–22.

[32] Sivandran Gajan, Bras Rafael L. Identifying the optimal spatially and temporally invariant root distribution for a semiarid environment. Water Resour Res 2012;48(12).

[33] Stephenson D, Shemang EM, Chaoka TR. Water Resources of Arid Areas: Proceedings of the International Conference on Water Resources of Arid and Semi-Arid Regions of Africa. Garborone, Botswana: Taylor & Francis; 2004 (3–6 August 2004).

[34] Genuchten van. A closed-form equation for predicting the hydraulic conductivity of unsaturated soils. Soil Sci Soc Am J 1980;44(5):892–8.

[35] Van Genuchten MTh, Gupta SK. A reassessment of the crop tolerance response function. Indian Soc Soil Sci 1993;41:730.

[36] Van Genuchten MT, U.S. Salinity Laboratory. A Numerical Model for Water and Solute Movement in and Below the Root Zone. United States Department of Agriculture Agricultural Research Service U.S. Salinity Laboratory 1987.

[37] van Wijk Mark T. Understanding plant rooting patterns in semi-arid systems: an integrated model analysis of climate, soil type and plant biomass. Global Ecol Biogeogr 2011;20(2):331–42.

[38] Vrugt JA, van Wijk MT, Hopmans JW, Simunek J. One-, two-, and three-dimensional root water uptake functions for transient modeling. Water Resour Res 2001;37(10):2457–70.

[39] Williams CA, Albertson JD. Soil moisture controls on canopy-scale water and carbon fluxes in an african savanna. Water Resour Res 2004;40(9).